Reprinted with permission from the publisher.
In: Science 2003. Vol. 299, pp. 1045–1048.
http://www.sciencemag.org/cgi/content/abstract/299/5609/1045

Low-Noise Current Amplifier Based on Mesoscopic Josephson Junction

J. Delahaye,[1]* J. Hassel,[2] R. Lindell,[1] M. Sillanpää,[1] M. Paalanen,[1] H. Seppä,[2] P. Hakonen[1]†

We used the band structure of a mesoscopic Josephson junction to construct low-noise amplifiers. By taking advantage of the quantum dynamics of a Josephson junction, i.e., the interplay of interlevel transitions and the Coulomb blockade of Cooper pairs, we created transistor-like devices, Bloch oscillating transistors, with considerable current gain and high-input impedance. In these transistors, the correlated supercurrent of Cooper pairs is controlled by a small base current made up of single electrons. Our devices reached current and power gains on the order of 30 and 5, respectively. The noise temperature was estimated to be around 1 kelvin, but noise temperatures of less than 0.1 kelvin can be realistically achieved. These devices provide quantum-electronic building blocks that will be useful at low temperatures in low-noise circuit applications with an intermediate impedance level.

Charge quantization in nanoelectronic devices is expected to lead to a variety of novel components. The most important invention so far is the single-electron transistor (SET) (*1, 2*), which presents an unsurpassed charge sensitivity both in the normal and superconducting states (*3*). Fast SETs are good candidates for readout devices in solid-state quantum computers (*4*). Owing to its small input capacitance, a SET works extremely well with large source impedances, and various applications of SETs have been proposed accordingly (*5*).

Superconducting quantum interference devices (SQUIDs) reach extremely good sensitivity with small-impedance sources (*6*). They are the common choice for measurements trying to approach the standard quantum limit or even attempting to go beyond it. At intermediate impedance values (~1 megohm), both SETs and SQUIDs run into problems due to impedance mismatch that seriously degrades their performance in this regime.

We present an experimental demonstration of a Bloch oscillating transistor (BOT) that is a good device candidate for intermediate impedance levels. The principle of the device (*7*) takes advantage of the interlevel transition probabilities and relaxation phenomena in a quantum Josephson junction (JJ), whereby it is possible to construct a device in which a small current of single electrons is used to generate a substantially larger (super)current of Cooper pairs. In our experiments, a ratio of more than 30 has been reached between these two currents.

The quantum behavior of a superconducting junction is described by the Schrödinger equation (*8*)

$$\frac{d^2\psi}{d(\varphi/2)^2} + \left(\frac{E}{E_C} + \frac{E_J}{E_C}\cos\varphi\right)\psi = 0 \qquad (1)$$

where ψ is the wave function describing the state of the JJ, E is energy, φ is the phase difference of the order parameter across the junction, $E_C = e^2/2C$ denotes the Coulomb energy set by the junction capacitance C, and the Josephson coupling energy $E_J = [(h/2\pi)/(2e)]I_C$ is given by the critical current I_C of the junction (h, Planck's constant; e, electronic charge). From this Mathieu equation, energy bands (Fig. 1) should be formed in a similar manner as that formed for electrons in a periodic potential (*9*). In the limit of small Josephson coupling, $E_J/E_C \ll 1$, the width of the lowest band is nearly equal to E_C, and the gap between the first and second bands is given by E_J. In the strongly superconducting case, $E_J/E_C \gg 1$, the bandwidth becomes exponentially small with $\exp[-(8E_J/E_C)^{1/2}]$, and the gap grows as $(8E_JE_C)^{1/2}$. This scenario is valid only if the quantum fluctuations of charge are suppressed by a resistance $R_C > R_Q = h/(2e)^2 \sim 6.5$ kilohms in the immediate vicinity of the junction (R_C, resistance of the environment; R_Q, quantum resistance); i.e., the lead capacitance is blocked off from the junction.

The basic quantum dynamics of a JJ involves Bloch oscillations and Zener tunneling (illustrated in Fig. 1, left). Bloch oscillations take place when the state of the junction adiabatically follows its ground state. Under the influence of a weak current bias, charge Q of the JJ runs along the band, which leads to Bloch reflection at the Brillouin zone boundary (indicated by the horizontal line in Fig. 1, left). This time-correlated tunneling of Cooper pairs is characterized by a frequency $f_B = I/2e$ in a current-biased JJ.

Zener tunneling occurs when the junction leaves its ground state at the Brillouin zone boundary by tunneling through the forbidden energy gap without a change of charge. As the bias current increases, the probability of crossing the band gap by Zener tunneling grows according to the formula ($E_J \ll E_C$)

$$P_{Zener} = \exp(-I_Z/I) \qquad (2)$$

where the Zener breakdown current $I_Z = \{(\pi eE_J^2)/[8(h/2\pi)E_C]\}$ (*10*). Thus, at bias currents $I \sim [(\pi E_J)/(16E_C)]I_C$, the probability of Zener tunneling becomes substantial.

Relaxation downward from higher bands can be induced either by an intrinsic mechanism at rate $\Gamma_\downarrow$ or by an external quasiparticle injection Γ_{ext}. If $\Gamma_\downarrow \ll \Gamma_{ext}$, then external, active control of the junction dynamics can be achieved. $\Gamma_\downarrow$ is a strong function of the environmental impedance R_C, and it can be made small when $R_C \gg R_Q$ and when temperature T is small (*11*).

To go beyond the regime of Coulomb

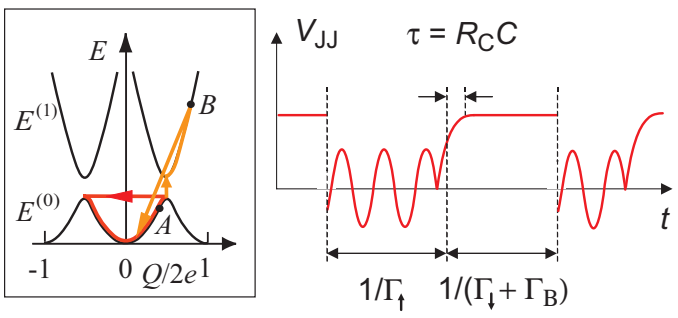

Fig. 1. Basic processes of a BOT in the charge space. (**Left**) Bloch oscillation on the lowest energy band $E^{(0)}$ is denoted by the closed red loop. Occasional Zener tunneling to the second band $E^{(1)}$ is marked by the vertical orange arrow, and the relaxation induced by external quasiparticle injection is indicated by the slanted orange arrow. On the lowest band, the largest possible voltage across the JJ is at point A, given by $V_{JJ}^{max} = dE^{(0)}/dQ|_{max}$; point B denotes the location where $V_{JJ} = V_{bias}$. (**Right**) The voltage of the Josephson junction (V_{JJ}) is displayed as a function of time. The upward and downward tunneling rates, $\Gamma_\uparrow$ and $\Gamma_\downarrow$, as well as the quasiparticle tunneling rate Γ_B are discussed in the text. A moving picture of the working cycle of the BOT can be found in Movie S1.

[1]Low Temperature Laboratory, Helsinki University of Technology, Post Office Box 2200, 02015 HUT, Finland. [2]Microsensing, VTT Information Technology, Post Office Box 1207, 02044 VTT, Finland.

*Present address: High Magnetic Field Laboratory, LCMI/CNRS BP 166, F-38042 Grenoble, France.
†To whom correspondence should be addressed. E-mail: pertti.hakonen@hut.fi

blockade of Cooper pairs (*12*) and to have a supercurrent I flowing in the JJ, the biasing voltage has to satisfy $V_{bias} > dE^{(0)}/dQ|_{max}$, the maximum slope of the lowest band (point A in Fig. 1, left). Then the junction will propagate along the lowest level and perform Bloch oscillations in a periodic manner at f_B. When the current increases, the probability of crossing the band gap by Zener tunneling grows. By properly selecting the ratio of E_J/E_C and the current I, one can tune the probability ratio P_{Zener}/P_{Bloch} so that the state of the junction will tunnel into the second band after a few Bloch oscillations (N on average).

If $V_{bias} < dE^{(1)}/dQ|_{max}$, the maximum slope of the second band, then the state of the JJ will become stationary on the higher band after Zener tunneling. If there is no intrinsic relaxation ($\Gamma_\downarrow \rightarrow 0$), the junction will not relax and it will remain stationary, i.e., Coulomb blockaded on the higher band (e.g., at point B in Fig. 1, left). Consequently, there will be no supercurrent in the JJ before relaxation takes place, owing to externally induced quasiparticle tunneling (indicated by the slanted orange arrow in Fig. 1, left). After relaxation, the junction will again resume the sequence of Bloch oscillations. In this way, a small current of injected quasiparticles results in a $2N$-amplified current of Cooper pairs. The voltage $V_{JJ}(t)$ over the JJ during the principal cycle of the BOT is illustrated in Fig. 1, right: $V_{JJ}(t)$ either varies sinusoidally at f_B or is fixed by V_{bias}. The transition from the former to the latter takes place over a time scale set by the R_CC time constant, whereas the opposite occurs within the electron tunneling time. The simplest realization of the BOT consists of a JJ, a normal metal tunnel junction (NIN), and a compact large resistance R_C (Fig. 2, top).

To estimate the current gain β of the BOT, we can incorporate the relaxation rate due to the base current I_B, $\Gamma_{ext} = \Gamma_B = I_B/e$, into the total downward transition rate [which becomes $\Gamma_\downarrow + \Gamma_B$ (Fig. 1, right)]. Assuming that the time constant for charge relaxation $\tau = R_CC$ can be neglected and that I_B flows only when the JJ is Coulomb blockaded, one may write for the BOT gain ($V_C > e/C$)

$$\beta = \frac{dI_C}{dI_B} = \frac{V_C}{eR_C}\,\frac{1}{\Gamma_\uparrow + \Gamma_\downarrow} \qquad (3)$$

Here I_C denotes the collector current and V_C is the total transport voltage. This equation predicts current gains on the order of 10 at $E_J/E_C = 0.7$ and $T = 0.1$ K. Further details can be found in (*13*).

We also performed more elaborate analysis of the BOT operation based on the application of $P(E)$ theory to the tunneling rates (*14*). The $P(E)$ theory takes into account probabilities of inelastic tunneling processes in a resistive environment where phase fluctuations are governed by R_C, and thereby, it allows us to simulate the operation of the BOT in a more reliable manner than was possible in the first simulations (*7*) based on the orthodox theory. By taking into account both the inelastic Cooper pair and quasiparticle tunneling, we obtained *I-V* curves similar to the measured ones. Contrary to Eq. 3, these simulations show that a small (on the order of 1 nA, strongly dependent on V_C) base current is needed to reach $\beta \sim 10$. According to our simulations, the maximum current gain takes place around $E_J/E_C \sim 1$, i.e., in a region where the approximations used ($E_J \ll E_C$) start to break down; hence, all the reported simulation results in this study should be considered as indicative only.

For technological reasons, our practical realization of the BOT is slightly different from the scheme shown in Fig. 2. Instead of the NIN junction for injecting quasiparticles, we used a superconductor-normal metal tunnel junction (SIN). This is a somewhat less desirable choice, but manufacturing such a device is nonetheless complicated because it requires a rather elaborate four-angle evaporation process (*15*). The sample structure consists of three elements: an Al-AlO_x-Al JJ [SQUID-like geometry for tunability (*15*)] with tunneling resistance $R_T^{JJ} \cong 5$ kilohms; a superconducting-normal Al-AlO_x-Cu tunnel junction with $R_T^{SIN} \cong 10$ kilohms; and a thin-film Cr resistor of $R_C \cong 50$ kilohms (20 μm long), located within a few μm of the two junctions. A scanning electron micrograph of a manufactured BOT device is displayed in Fig. 2, bottom.

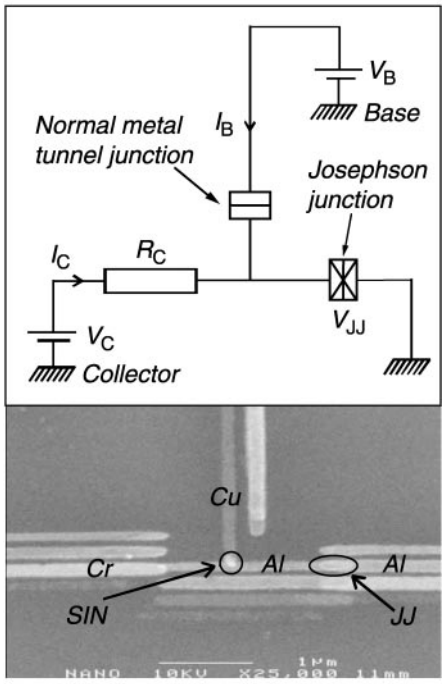

Fig. 2. (**Top**) Implementation of a Bloch oscillating transistor. R_C denotes the collector resistance; bias currents and the corresponding voltage sources are also marked. (**Bottom**) A scanning electron micrograph of a manufactured device in which the normal metal tunnel junction has been replaced by a SIN (Al-AlO_x-Cu) tunnel junction.

The measured *I-V* characteristics of a hysteretic BOT device, called H, are illustrated (Fig. 3) at a few values of base current I_B. The voltage V_C denotes the full voltage across the Cr resistor and the JJ. The base current to the SIN junction is injected by means of a 100-megohm bias resistor at room temperature, but this biasing effectively becomes a voltage bias owing to the line capacitance of the coaxial line inside the cryostat. The active region, where I_B has a large effect, is small and moves with increasing I_B. The *I-V* curves are slightly hysteretic with respect to the direction of the voltage ramp; of our three samples, only sample H (*15*) showed hysteresis. The hysteresis is related to the fact that a variable part of I_B causes only intraband transitions, not relaxation from the upper level.

There is a substantial asymmetry with respect to the polarity of V_C in the *I-V* curves of sample H (the region where $|V_C|$ is slightly below the hysteresis loop in Fig. 3). At $I_B = +0.8 \ldots +1.2$ nA, the maximum current-induced change at $V_C < 0$ is ~10 times that at $V_C > 0$. We consider this asymmetry as very strong proof that the underlying principle of the BOT operation is working: Relaxation due to quasiparticle tunneling can take place only under one polarity (*16*). If the device would work as a parametric amplifier owing to I_B-induced changes in the environmental impedance, then the behavior should be symmetric. The maximum current gain is

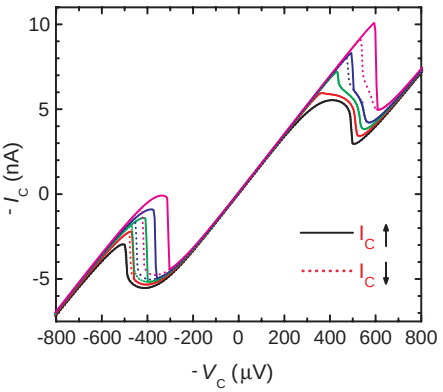

Fig. 3. Current-voltage characteristics for a hysteretic BOT device (sample H) at base current $I_B = 0$ (black), 0.4 nA (red), 0.8 nA (green), 1.2 nA (blue), and 2 nA (magenta). The parameters of the device are as follows: $E_J = 78$ μeV, $E_C = 50$ μeV, $R_C = 54$ kilohms, $R_T^{JJ} = 7.7$ kilohms, and $R_T^{SIN} = 5.8$ kilohms, where R_T^{JJ} and R_T^{SIN} refer to the resistances of the Josephson and SIN junctions, respectively. Up and down voltage sweeps are represented by the solid and dotted curves, respectively.

obtained at $I_B = 1$ nA, which is consistent with our simulations using $P(E)$ theory.

In the measured current gain at $I_B = 1$ nA on a nonhysteretic sample (NH) (Fig. 4), the gain is seen to peak rather strongly with respect to the transport voltage; the peaking of the current gain becomes more prominent with increasing values of β. This peaking reflects the strong dependence of Zener tunneling on the external current. However, negative feedback can always be used to enhance the operating region.

As a function of E_J/E_C, we find a maximum, $\beta \sim 35$, at an optimum ratio of $E_J/E_C = 3.4$. Such a large ratio for E_J/E_C means that higher bands of the junction are involved in the process: The lowest bands are too narrow to present a Coulomb blockade that is as large as that needed for the BOT operation. This factor has not yet been taken into account in our simulations. Above the optimum ratio, the gain drops quickly. At present, the rapid decrease of gain at large values of E_J/E_C is not understood, and it may be a weakness of our nonoptimized first devices.

The other main characteristics of a low-noise amplifier are the available power gain η, the bandwidth BW, the dynamic range A, the optimum input impedance Z_{opt}, and the noise temperature T_N. For the available power gain of sample NH, we obtained a value of $\eta = [(Z_{out})/(Z_{in})]\beta^2 = 5$ by measuring β, Z_{in}, and Z_{out}. This small value is due to an impedance conversion, i.e., the measured input impedance follows $Z_{in} \cong \beta R_C$, whereas at the output, $Z_{out} = -30$ kilohms at the optimum operating point. The bandwidth is expected to be limited well below $\min(1/R_CC, f_B/\beta) \sim 1$ GHz, set either by the RC time constant or the Bloch oscillation frequency. The bandwidth restricts the minimum value of I_B because, at least, $I_B > 2eBW$, according to the Nyquist sampling theorem. From the experimental curves in Fig. 4, we obtain for the dynamic range $A = 50$ pA at the largest current gains. At gains on the order of 10, $A = 250$ pA.

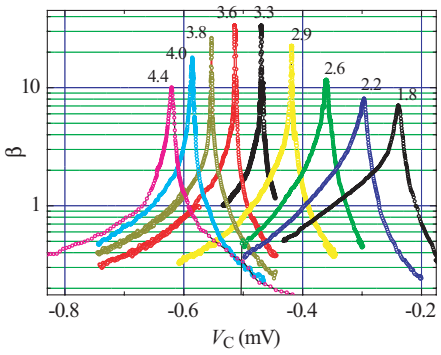

Fig. 4. Current gain measured for a nonhysteretic BOT (sample NH) when the ratio E_J/E_C is tuned over 1.8 to 4.4. The base current was fixed at $I_B = 1$ nA to maximize the current gain. The parameters of the device are as follows: $E_J^{max} = 150$ μeV, $E_C = 35$ μeV, $R_C = 67$ kilohms, $R_T^{JJ} = 4.3$ kilohms, and $R_T^{SIN} = 10$ kilohms. In this BOT, we also had a Cr resistor of 50 kilohms next to the SIN junction.

The noise properties of a BOT are rather complicated. This is mostly because the input and output noises are strongly correlated. Consequently, our noise analysis differs slightly from the standard modeling. A BOT has two principal noise sources: the shot noise due to I_B and the broadening of the Bloch oscillation peak caused by the current fluctuations in collector resistance R_C. Owing to charge relaxation through R_C, a BOT is insensitive to $1/f$ background charge fluctuations that severely hamper the operation of SETs.

The width of the Bloch oscillation peak is given by the equation (*8*)

$$\Gamma_B = (\pi/e)^2 k_B T/R_C \qquad (4)$$

This contribution spreads approximately over the frequency span of 2 GHz at $T = 100$ mK with $R_C = 67$ kilohms. Thus, even though the total power of the Bloch oscillation peak was as high as $(100\ \mu eV)^2$, it amounts only to voltage noise of 2 nV/(Hz)$^{1/2}$. Further away from f_B, its contribution becomes smaller, and its share can be neglected below 1 GHz; indeed, the Bloch peak is so weak and broad that it is barely visible in the Fourier power spectra of our simulated data.

The most detrimental noise contribution is the current fluctuation i_n due to the shot noise of I_B (*17*). Because it is inherent to the device owing to tunneling of electrons at the base, this noise component must be independent of the source impedance. In our noise model, the source independence is achieved with a correlated voltage noise generator, $e_n = Z_{in}i_n$, in the input circuit. Optimization with respect to the noise factor (*18*) results in $Z_{opt} = Z_{in}$ and $T_n = Z_{in}i_n^2/k_B = 2eI_BZ_{in}/k_B \sim eV_{in}/k_B$. Typical values for our present samples are $Z_{opt} =$ 300 to 400 kilohms and $T_n = 1$ to 4 K, calculated for moderate current gains of $\beta =$ 4 to 6 at $I_B = 0.2$ to 0.4 nA [$i_n \sim 8$ to 11 fA/(Hz)$^{1/2}$] (*19*). With $i_n = 10$ fA/(Hz)$^{1/2}$, the relative dynamic range becomes better than 80 dB/(Hz)$^{1/2}$.

T_n may be substantially smaller than the above estimate. According to our simulations, the base current consists of two parts: $I_B = I_{B1} + I_{B2}$, where I_{B1} induces interlevel transitions (relaxation), whereas I_{B2} causes transitions within only one band. The ratio I_{B1}/I_{B2} depends on the operating point and, typically, we find $I_{B2} > I_{B1}$ in our calculations. Because only I_{B1} produces current gain, we expect $T_n^{calc} \sim 2eI_{B1}Z_{in}/k_B \ll T_n$. In the hysteretic regime, which vanishes with growing resistance of the base tunnel junction, the ratio I_{B1}/I_{B2} has two stable values. Close to the hysteretic region, the devices have a large gain, because, in addition to the change of I_B, there will be an enhancement in output current owing to a change in I_{B1}/I_{B2}.

In principle, a BOT can be used as a voltage-triggered, single-shot detector at $I_B = 0$. In this mode, a pair of oppositely biased BOTs can be used as an "event trigger" detector for charge qubits (*20*). Unfortunately, only a very small coupling between the qubit and the BOT is tolerated if one wants to equal the decoherence times measured recently by Vion *et al.* (*21*).

The most likely application of the BOT will be a submillimeter-wave detector based on either a SIN (*22*) or a SIS (superconductor-insulator superconductor) tunnel junction (*23*). Based on a SQUID readout with a noise of 50 fA/(Hz)$^{1/2}$ (*24*), a SIN detector reaches a noise-equivalent power of 10^{-18} W/(Hz)$^{1/2}$. Similar noise characteristics are obtained with SIS detectors, for which SET readouts have been demonstrated to yield $i_n = 15$ fA/(Hz)$^{1/2}$ (*25*). Our noise estimates for BOTs compare well with these results, even though they are based on first, nonoptimal devices. It has been suggested (*25*) that single-photon counting could be implemented with a quantum-limited SET for readout. An optimized BOT might reach the same performance, but in this case, it might be better to use a BOT as a charge multiplier, i.e., in a mode where individual charge pulses in the output are resolved.

BOTs may also find their way into metrology, where the detection and comparison of small quantized currents generated by a single-electron tunneling current pump is an issue. Ultimately, the goal is to close the quantum triangle by combining Josephson voltage, quantum Hall resistance, and quantum current standards at the level of relative uncertainty of 10^{-8}. One approach is to use an amplifier based on a cryogenic current comparator and a SQUID to multiply the current generated by a SET pump. The equivalent current noise for such a setup has been demonstrated to be 4 fA/(Hz)$^{1/2}$ (*26*). With a BOT, one should reach comparable noise levels, with the further benefit of an on-chip integration of the readout element.

References and Notes

1. D. V. Averin, K. K. Likharev, *J. Low Temp. Phys.* **62**, 345 (1986).
2. T. A. Fulton, G. J. Dolan, *Phys. Rev. Lett.* **59**, 109 (1987).
3. A. Aassime, D. Gunnarsson, K. Bladh, P. Delsing, R. Schoelkopf, *Appl. Phys. Lett.* **79**, 4031 (2001).
4. M. H. Devoret, R. J. Schoelkopf, *Nature* **406**, 1039 (2000).
5. K. K. Likharev, *Proc. IEEE* **87**, 606 (1999).
6. J. Clarke, in *SQUID Sensors: Fundamentals, Fabrication, and Applications*, H. Weinstock, Ed. (Kluwer Academic, Amsterdam, 1996), pp. 1–62.
7. J. Hassel, H. Seppä, *IEEE Trans. Appl. Supercond.* **11**, 260 (2001).
8. D. Averin, K. K. Likharev, A. B. Zorin, *Sov. Phys. JETP* **61**, 407 (1985).
9. See, for example, G. Schön, A. D. Zaikin, *Phys. Rep.* **198**, 237 (1990).
10. A. D. Zaikin, I. N. Kosarev, *Phys. Lett. A* **131**, 125 (1988).

11. A. D. Zaikin, D. S. Golubev, *Phys. Lett. A* **164**, 337 (1992).
12. D. B. Haviland, L. S. Kuzmin, P. Delsing, T. Claeson, *Europhys. Lett.* **16**, 103 (1991).
13. J. Delahaye *et al.*, *Physica E*, in press.
14. G. L. Ingold, Yu. V. Nazarov, in *Single Charge Tunneling, Coulomb Blockade Phenomena in Nanostructures*, H. Grabert, M. Devoret, Eds. (Plenum, New York, 1992), pp. 21–107.
15. Materials and methods are available as supporting material on *Science* Online.
16. If quasiparticle tunneling occurs in the opposite direction, the tunneling brings the junction charge Q further away from the background charge Q_0, and the energy will increase according to $[1/(2C)](Q - Q_0)^2$. Consequently, the junction will make a transition to the third energy level.
17. The output current is made of charge pulses of size βe. Therefore, the output current noise is given by $[2(\beta e)I_{out}]^{1/2} = [2(\beta e)\beta I_B]^{1/2} = \beta[(2eI_B)^{1/2}]$, and this reduces to the shot noise of I_B at the input. This contains all of the noise, except possible leakage current contributions. The apparent switching voltage noise at the output is given simply by the instantaneous $R_C I_{out}(t)$.
18. A. van der Ziel, *Noise in Solid State Devices and Circuits* (Wiley, New York, 1986), chap. 3.
19. There is a small noise contribution from the output leakage current of $\sim$1 nA. Using the measured transconductance $g_m \cong 1/R_C$ (valid when $\beta > 5$), we estimate a contribution of 0.4 K in T_n.
20. Yu. Makhlin, A. Schnirman, G. Schön, *Rev. Mod. Phys.* **73**, 357 (2001).
21. D. Vion *et al.*, *Science* **296**, 886 (2002).
22. M. Nahum, J. M. Martinis, *Appl. Phys. Lett.* **63**, 3075 (1993).
23. A. Peacock *et al.*, *Nature* **381**, 135 (1996).
24. See, for example, D. Golubev, L. Kuzmin, *J. Appl. Phys.* **89**, 6464 (2001).
25. R. J. Schoelkopf, S. H. Moseley, C. M. Stahle, P. Wahlgren, P. Delsing, *IEEE Trans. Appl. Supercond.* **9**, 2935 (1999).
26. Y. De Wilde, F. Gay, P. M. Piquemal, G. Génevès, *IEEE Trans. Instrum. Meas.* **50**, 231 (2001).

27. We acknowledge interesting discussions with M. Kiviranta, J. Pekola, J. Penttilä, A. Schakel, and A. D. Zaikin. This work was supported by the Academy of Finland and by the Large Scale Installation Program ULTI-3 of the European Union (HPRI-CT-1999-00050).

Supporting Online Material

www.sciencemag.org/cgi/content/full/299/5609/1045/DC1
Materials and Methods
Table S1
Reference
Movie S1

16 October 2002; accepted 20 December 2002